Electron optics with magnetic vector potential barriers in graphene

2009 J. Phys.: Condens. Matter 21 292204

(http://iopscience.iop.org/0953-8984/21/29/292204)

IOP FTC
IOP PUBLISHING JOURNAL OF PHYSICS: CONDENSED MATTER
J. Phys.: Condens. Matter **21** (2009) 292204 (8pp) doi:10.1088/0953-8984/21/29/292204

FAST TRACK COMMUNICATION

Electron optics with magnetic vector potential barriers in graphene

Sankalpa Ghosh[1] **and Manish Sharma**[2]

[1] Department of Physics, Indian Institute of Technology, Delhi, New Delhi-110016, India
[2] Centre for Applied Research in Electronics, Indian Institute of Technology, Delhi, New Delhi-110016, India

Received 16 March 2009, in final form 19 May 2009
Published 3 July 2009
Online at stacks.iop.org/JPhysCM/21/292204

Abstract
An analysis of electron transport in graphene in the presence of various arrangements of delta-function like magnetic barriers is presented. The motion through one such barrier gives an unusual non-specular refraction leading to asymmetric transmission. The symmetry is restored by putting two such barriers in opposite directions side by side. Periodic arrangements of such barriers can be used as Bragg reflectors whose reflectivity has been calculated using a transfer matrix formalism. Such Bragg reflectors can be used to make resonant cavities. We also analyze the associated band structure for the case of infinite periodic structures.

(Some figures in this article are in colour only in the electronic version)

In a two-dimensional electron gas (2DEG) there is a well established similarity between ballistic electron transport through electrostatic potential barriers and light propagation in geometrical optics [1]. This has been extended to massless Dirac fermions in graphene [2, 3], where it was recently established that electron transport in the presence of an electrostatic potential barrier is analogous to negative refraction through metamaterials [4, 5]. The relativistic behavior of graphene electrons also leads to Klein tunneling [6, 7], where a relativistic particle can tunnel through a high barrier by the process of pair production, precluding the possibility of confining it using such potential barriers. Such confinement is, however, possible using magnetic barriers [8]. Can we understand this behavior of massless Dirac fermions in the presence of magnetic barriers by comparing it to the propagation of light? The difficulty in using an optical analogy is that, unlike the electrostatic potential, the magnetic vector potential couples with the momentum of the electron.

In this work we show that wavevector dependent tunneling of massless Dirac fermions through magnetic barriers [9–14] can be understood in terms of well-known ideas in geometrical optics. However, the corresponding Snell's laws are very different from those of ordinary geometrical optics. We then carry out this analysis to propose devices such as a Bragg reflector using a transfer matrix approach and qualitatively depict how a resonant cavity can be constructed with such a reflector. Additionally, we comment on the band structure of electron transport when such magnetic barriers are placed periodically.

The proposed structure consists of a graphene sheet placed in close proximity to long magnetic stripes that produce highly localized magnetic fields, as depicted in figure 1. Such field profiles can be created using demagnetizing fields produced at the edges of narrow stripes made with hard ferromagnetic materials with perpendicular or in-plane anisotropy. It is possible to make such stripes at various length scales. Materials such as CoCrPt, used in magnetic recording, produce field strengths of 1 T close to the surface with bit lengths ranging from 50 to 100 nm. Patterned stripes down to 10 nm can be realized using nanolithography [15]. It is possible to achieve field profiles at even smaller dimensions using domain walls with widths in the range of 10–50 nm and magnetic nanostructures down to 5 nm [16, 17] and 0.15 nm [18] having highly localized field variations. The particular form of magnetic barrier that is used in the calculation here can be realized using two narrow ferromagnetic stripes of perpendicular anisotropy with appropriately narrow dimensions and magnetized in opposite directions (figure 1(a)). The same profile can also be achieved with one ferromagnetic stripe whose magnetization is parallel to the graphene sheet at a height z_0 above it (figure 1(b)). Such barriers have been used in the literature [9–11] and the

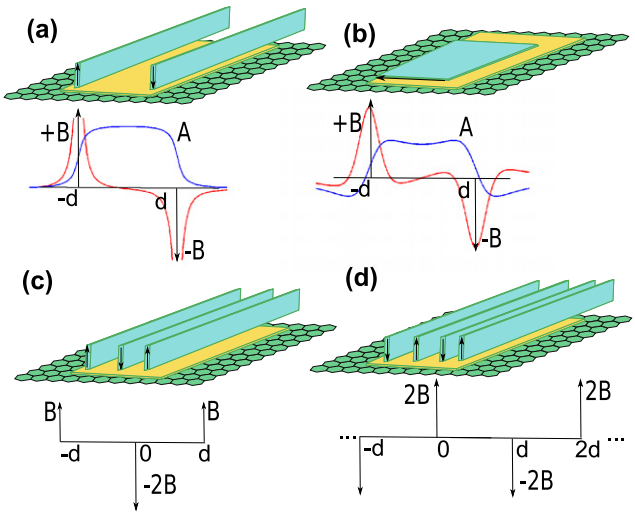

Figure 1. Monolayer graphene with ferromagnetic stripes having magnetizations perpendicular (a) and parallel (b) to the plane. The magnetic field B produces a magnetic vector potential A. Single MVP barriers are formed in (a) and (b). Also shown are a double MVP barrier (c) and a periodic lattice (d).

magnetic field of such structures is

$$\boldsymbol{B} = B(x, z_0)\hat{z} = B_0[K(x + d, z_0) - K(x - d, z_0)]\hat{z}.$$

Here, $K(x, z_0) = -\frac{2z_0 d}{x^2+z_0^2}$ and B_0 is a constant dependent on the aspect ratio of the stripe. Figure 1(a) shows a plot the profile of such a magnetic field and the corresponding vector potential for a given value of z_0. As the plot shows, such an inhomogeneous magnetic field can be well approximated as a delta-function-like magnetic barrier. This approximation is valid for all the different sized geometries discussed in the preceding paragraph as long as two length scales are satisfied. The first is the typical magnetic length $\ell_B = \sqrt{\frac{\hbar c}{|e|B}}$, which is of the order of the width of such magnetic barriers. The second length scale is dictated by the de Broglie wavelength, λ_F, of the electron. The scattering states in the presence of such barriers are generally characterized by $\lambda_F \sim 1/k_F$, where k_F is the Fermi wavevector. As long as λ_F is much larger than the typical width of the magnetic barriers, the electrons will not see the variation in the vector potential and thus the delta-function approximation will hold. Accordingly, we use such delta-function-like barriers in the rest of the paper. This choice is guided by the fact that it is amenable to simpler mathematical treatment, thus making the optical analogy more transparent. We shall, however, point out later that the discussed analogy with geometrical optics is more general and is applicable for other types of magnetic barrier with finite width [8].

We use the following magnetic field and vector potential in the Landau gauge for a magnetic potential barrier [9, 10]:

$$\boldsymbol{B} = B\ell_B[\delta(x + d) - \delta(x - d)]\hat{z};$$

$$\boldsymbol{A}_y(x) = B\ell_B\Theta(d^2 - x^2)\hat{y}.$$

Since $\Theta(x)$ is the Heaviside step function, we call this a magnetic vector potential (MVP) barrier.

For massless Dirac fermions in graphene in MVP barriers, we consider the limit where the electrons at the K and K' points are decoupled from each other [19]. This approximation will break down if the change in the wavevector $|K - K'| \geqslant 2k_F$ due to scattering [3]. For the magnetic barriers considered in this paper, this shift is $\sim|1/l_B|$. For fields $\sim$1 T, it is found that $|1/l_B| < 2k_F$, and thus this approximation holds. Near each such point, the wavefunction is given by a two-component spinor and satisfies the equation

$$v_F(\pi_x \pm i\pi_y)\psi_{2,1} = E\psi_{1,2}. \tag{1}$$

Here, v_F is the Fermi velocity ($\approx c/300$) and $\boldsymbol{\pi} = \boldsymbol{p} + \frac{e}{c}\boldsymbol{A}$. Using $\frac{\hbar v_F}{\ell_B}$ as the unit of energy such that $\epsilon = \frac{E\ell_B}{\hbar v_F}$, ℓ_B as the unit of the length such that $\bar{x} = \frac{x}{\ell_B}$, $\mathrm{sgn}(e) = -1$ and $\psi = \phi(x)e^{ik_y y}$ in the Landau gauge, we get

$$-i\left[\frac{\partial}{\partial\bar{x}} \pm (k_y\ell_B - \Delta)\right]\phi_{2,1} = \epsilon\phi_{1,2}. \tag{2}$$

Here, $\Delta = 1$ for $|x| < d$ and $=0$ for $|x| > d$. The above two coupled equations can be decoupled easily and result in a Schrödinger like equation of the form

$$\left[-\frac{\partial^2}{\partial\bar{x}^2} + (k_y\ell_B - \Delta)^2\right]\phi_{1,2} = \epsilon^2\phi_{1,2}.$$

In the region $-d < x < d$ electrons see a barrier of height $[k_y + \mathrm{sgn}(e)\frac{1}{\ell_B}]^2$. The corresponding wavefunctions in any region of space can be written in terms of a linear superposition of forward and backward moving plane waves such that

$$\phi_1 = \begin{cases} e^{ik_x x} + re^{-ik_x x} & x < -d \\ ae^{iq_x x} + be^{-iq_x x} & |x| < d \\ te^{ik_x x} & x > d \end{cases} \tag{3}$$

$$\phi_2 = \begin{cases} s[e^{i(k_x x+\phi)} - re^{-i(k_x x+\phi)}] & x < -d \\ s'[ae^{i(q_x x+\theta)} - be^{-i(q_x x+\theta)}] & |x| < d \\ ste^{i(k_x x+\phi)} & x > d. \end{cases} \tag{4}$$

Solutions of the above equations are very different from those in the presence of a uniform magnetic field, since here the magnetic field is highly non-uniform and has singular delta-function-like structures. Also, s and s' are given by $\mathrm{sgn}(\epsilon)$ and are both $+1$ for electrons when only magnetic fields are present and no electrostatic potentials are applied. A similar treatment can be done in the presence of an additional electrostatic potential, in which case both s and s' are not necessarily $+1$ [20]. The wavevector components are $[k_x, k_y] = k_F[\cos\phi, \sin\phi]$ outside the magnetic barrier and ϕ is the incident angle for an electron wave. The Fermi energy of the incident electrons is $E_F = \hbar v_F k_F$. In the dimensionless form, this is $\epsilon_F = k_F\ell_B$ and this entirely characterizes the parameters that control the transport by changing the refractive index of the barrier region. Since the magnetic field does not do any work, energy conservation gives $k_x^2 + k_y^2 = k_F^2$ for $|x| > d$ and $q_x^2 + (k_y - \frac{1}{\ell_B})^2 = k_F^2$ for $|x| < d$. Since $\theta = \cos^{-1}(\frac{q_x}{k_F})$, for $|x| < d$ $k_F \sin\theta = k_y - \frac{1}{\ell_B}$ gives

$$\sin|\theta| = \sin|\phi| - \mathrm{sgn}(\phi)\frac{1}{k_F\ell_B}, \qquad -\frac{\pi}{2} < \phi < \frac{\pi}{2}. \tag{5}$$

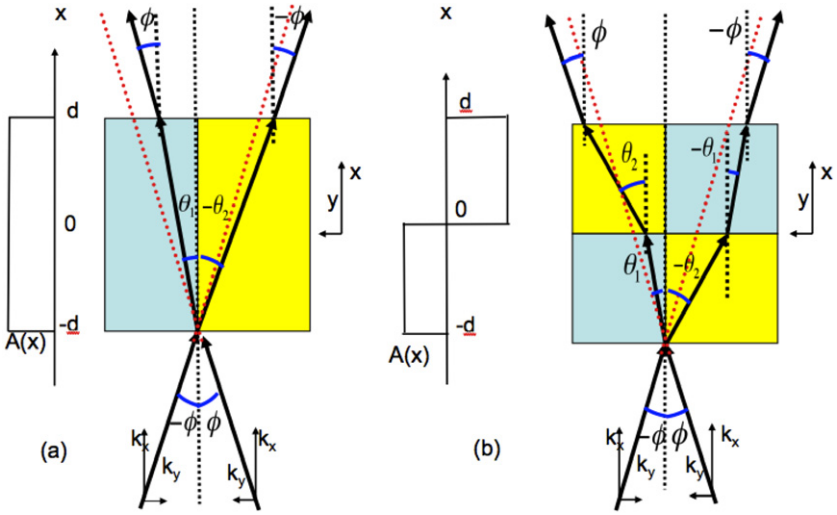

Figure 2. (a) Asymmetric refraction through a single barrier. (b) Refraction through a double barrier where the symmetry in the transmission is restored. Barrier regions which are denser or rarer in terms of refraction of the wavevector are shaded differently.

The situation has been depicted in figure 2(a). The wave incident with a positive ϕ wavevector will bend towards the normal, whereas for the waves incident with negative incidence angle the corresponding wavevector will bend away from the surface normal inside the barrier region. Therefore, Snell's law of electron waves in such magnetic barriers is not specular as it is for light waves on a smooth surface or for the incidence of electrons on an electrostatic potential barrier [4, 6]. This unusual refraction can also be thought of as a consequence of breaking time reversal symmetry in the presence of such magnetic barriers. When the magnetic field is reversed, the denser and rarer medium will change sides without changing the asymmetric transmission.

According to equation (5), when $|\sin|\theta|| > 1$, θ becomes imaginary and the wave in the second medium becomes evanescent. In the language of optics this corresponds to total internal reflection (TIR). According to figure 2(a), this will happen when $\sin|\theta| > 1$ for $-\frac{\pi}{2} \leqslant \phi < 0$ and when $\sin|\theta| < -1$ for $0 < \phi \leqslant \frac{\pi}{2}$. In the latter case, this requires the wavevector to be negatively refracted [4] at a sufficiently high magnetic field before TIR occurs. It also follows that for a given strength B the magnitude of the critical angle of incidence $|\phi| = \phi_c$ for TIR is higher for $0 < \phi < \frac{\pi}{2}$ compared to the value for $-\frac{\pi}{2} \leqslant \phi < 0$. Because of TIR the transmission on both sides of figure 3 drops to 0 beyond a certain value of ϕ and this value is lower for negative angles of incidence.

The wavefunctions given in equations (3) and (4) are similar to those of massless Dirac electrons scattered by an electrostatic step potential considered in [6]. This is because the MVP barrier creates a momentum dependent step potential of $[k_y + \mathrm{sgn}(e)\frac{1}{\ell_B}]^2$. Continuity of the wavefunction at the boundaries of the MVP barrier can be used to calculate the transmission coefficient as

$$t = \frac{2ss'\mathrm{e}^{-\mathrm{i}k_x D}\cos\phi\cos\theta}{ss'[\mathrm{e}^{-\mathrm{i}q_x D}\cos(\phi+\theta) + \mathrm{e}^{\mathrm{i}q_x D}\cos(\phi-\theta)] - 2\mathrm{i}\sin q_x D}. \quad (6)$$

Here $D = 2d$. Thus, the transmission coefficient t, transmittance $T = t^*t$ and reflectance $R = 1 - T$ have same expressions as for electrostatic potentials in [6].

There are, however, key differences. For an electrostatic barrier, as $\phi \to -\phi, \theta \to -\theta$. For a magnetic barrier, because of equation (5), this is not the case. Thus, the same equation (6) gives symmetric transmission for an electrostatic potential in [6] and asymmetric transmission here. For high electrostatic barriers, such that $V \gg E_F$, the wavevector is given by $q_x = \sqrt{\frac{(E_F-V)^2}{\hbar^2 v_F^2} - k_y^2}$, which is real. The corresponding transmittance for electrostatic potentials is

$$T = \frac{\cos^2\phi}{1 - \cos(q_x D)\sin^2\phi} \quad (7)$$

and is 1 at $\phi = 0$. This exhibits Klein tunneling for massless Dirac fermions [6]. For the magnetic barrier, $\frac{1}{k_F \ell_B} \propto \sqrt{B}$. However, unlike the electrostatic field case, application of a magnetic field changes both components of the wavevector but not the energy. At high magnetic field, $q_x^2 = k_F^2 - (k_y - \frac{1}{\ell_B})^2 = -\kappa^2 < 0$. As discussed, this leads to TIR and not Klein tunneling. In figure 3, the magnitude of critical angle beyond which TIR occurs is lower for a higher magnetic field. Then, a stronger MVP barrier leads to higher reflections as opposed to complete transmission at normal incidence by a high electrostatic potential barrier. A similar situation is encountered with other forms of magnetic barrier [8, 21].

Complete transmission only occurs for $q_x D = n\pi$ in equation (6). This corresponds to resonant tunneling for Dirac electrons and happens in the same way as for non-relativistic electrons, appearing as a number of peaks in the plots in figure 3. The number of such tunneling peaks increases with barrier width for both MVP barriers and electrostatic barriers.

Recently, Masir *et al* [13, 14] considered the problem of transport through magnetic barriers including the single MVP barriers discussed here. They have also compared their results with similar transport for non-relativistic electrons having a

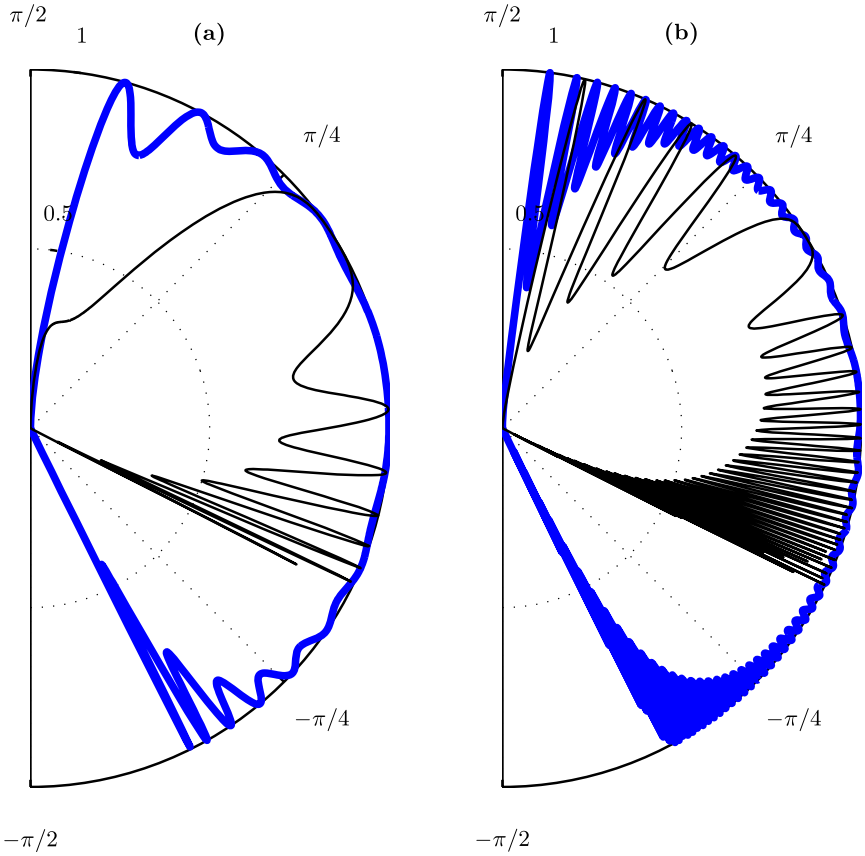

Figure 3. Polar plot of T versus ϕ for single MVP barriers of widths (a) 100 nm and (b) 500 nm. Blue (thick) = 0.1 T with $l_B = 81$ nm, Black (thin) = 3 T with $l_B = 14.8$ nm.

parabolic spectrum and found that there are a larger number of resonant tunneling peaks for massless Dirac fermions and they are also more pronounced. However, the structures discussed in [13, 14] give only asymmetric transmission.

To get symmetric transmission out of such a barrier, two such single MVP barriers could be placed side by side but oppositely oriented, as depicted in figure 1(c). The magnetic field creating such a barrier is

$$\boldsymbol{B} = B_z(x)\hat{z} = B\ell_B[\delta(x+d) + \delta(x-d) - 2B\delta(x)]\hat{z}.$$

We again consider energy conservation in medium 1 ($-d < x < 0$) and medium 2 ($0 < x < d$), which gives

$$\begin{aligned} q_{1,2}^2 + \left(k_y \mp \frac{1}{\ell_B}\right)^2 &= k_{\mathrm{F}}^2; \\ \sin|\theta_{1,2}| = \sin|\phi| &\mp \mathrm{sgn}(\phi)\frac{1}{k_{\mathrm{F}}\ell_B}. \end{aligned} \tag{8}$$

The angle if incidence is $-\frac{\pi}{2} < \phi < \frac{\pi}{2}$ and the angle of refraction is θ_1 and θ_2 in media 1 and 2 respectively. The absolute value of the relative refractive index of region 1 with respect to region 2 on the left side of the surface normal is just the inverse of that on the right side of the surface normal and can be combined in the following expression:

$$|_1 n_2| = \frac{\sin|\theta_1|}{\sin|\theta_2|} = \frac{\sin|\phi| - \mathrm{sgn}(\phi)\frac{1}{k_{\mathrm{F}}\ell_B}}{\sin|\phi| + \mathrm{sgn}(\phi)\frac{1}{k_{\mathrm{F}}\ell_B}}. \tag{9}$$

Thus, for such double MVP (DMVP) barriers, the wavevector bending towards (away from) the surface normal in the first half of the barrier bends away from (towards) the surface normal in the second half of the barrier, as shown in figure 2(b). This will achieve symmetric transmission through such a barrier as demonstrated in figure 4. Critical angles of incidence beyond which TIR will occur for positive and negative ϕ will also be interchanged when going from the first to the second barrier region. However, at higher B fields, TIR will occur at both regions of the barrier. Consequently, the total reflectivity of the barrier increases, as can be seen by comparing figures 3 and 4.

Very recently, a similar problem of transport was considered but for finite-width magnetic barriers [22]. The relevant results in that work are similar to the present case of delta-function barriers. This suggests that the conclusions for symmetric and asymmetric transmission continue to hold true for finite-width barriers as well.

Practical devices such as Bragg reflectors can be made by exploiting the high reflectivity of DMVP barriers to manipulate electrons, as will be discussed later. Such structures, if

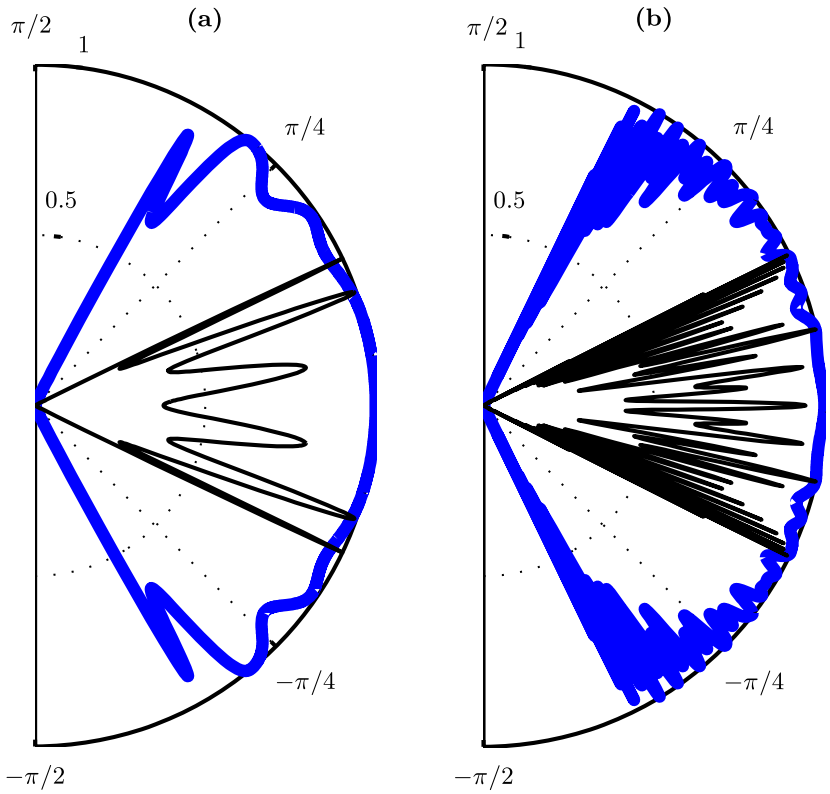

Figure 4. Polar plot of T versus ϕ for DMVP barriers of widths (a) 100 nm, (b) 500 nm. Blue (thick) = 0.1 T with $l_B = 81$ nm, Black (thin) = 3 T with $l_B = 14.8$ nm.

realized, could also be very useful for confining carriers in desired areas in graphene and away from edges, where edge states could adversely affect transport.

To calculate transmittance for DMVP barriers, we write the wavefunction in the same way as in equations (3) and (4):

$$\phi_1 = \begin{cases} e^{ik_x x} + re^{-ik_x x} & x < -d \\ ae^{iq_1 x} + be^{-iq_1 x} & x \in [-d, 0] \\ ce^{iq_2 x} + de^{-iq_2 x} & x \in [0, d] \\ te^{ik_x x} & x > d \end{cases} \tag{10}$$

$$\phi_2 = \begin{cases} s[e^{i(k_x x+\phi)} - re^{-i(k_x x+\phi)}] & x < -d \\ s_1[ae^{i(q_1 x+\theta_1)} - be^{-i(q_1 x+\theta_1)}] & x \in [-d, 0] \\ s_2[ce^{i(q_2 x+\theta_2)} - de^{-i(q_2 x+\theta_2)}] & x \in [0, d] \\ ste^{i(k_x x+\phi)} & x > d. \end{cases} \tag{11}$$

The corresponding sign factors associated with ϕ_2 in these regions are s_1 and s_2 and are both 1. The transmittance and reflectance can now be easily computed by imposing the continuity conditions on the above functions at the locations of the barriers, namely at $x = -d, 0, d$. We can express the transmittance and reflectance in a compact form by introducing $A = e^{-ik_x x}$ and $B_{1,2} = e^{-iq_{1,2} x}$ to define the following matrices:

$$M_A = \begin{bmatrix} A & 0 \\ 0 & A^* \end{bmatrix}, \qquad M_{\theta_{1,2},\phi} = \begin{bmatrix} 1 & 1 \\ e^{i\theta_{1,2},\phi} & -e^{-i\theta_{1,2},\phi} \end{bmatrix}$$

$$M_{s,s_1,s_2} = \begin{bmatrix} 1 & 0 \\ 0 & s, s_1, s_2 \end{bmatrix} = I, \qquad M_{B_{1,2}} = \begin{bmatrix} B_{1,2} & 0 \\ 0 & B_{1,2}^* \end{bmatrix}.$$

Here I is the unit matrix and

$$M_A^{-1} = M_A^*; \qquad M_{B_{12}}^{-1} = M_{B_{12}}^*. \tag{12}$$

The solution of these continuity equations can then be written as

$$[\,1 \quad r\,]^{\mathrm{T}} = M_A^* {M_\phi}^{-1} [M_{\theta_1} M_{B_1} M_{\theta_1}^{-1} M_{\theta_2} M_{B_2} M_{\theta_2}^{-1}] M_\phi M_{A^*} [\,t \quad 0\,]^{\mathrm{T}}.$$

To understand the above formulae, we introduce the transfer matrix through a DMVP barrier:

$$T_{\mathrm{DMVP}} = M_{\theta_1} M_{B_1} M_{\theta_1}^{-1} M_{\theta_2} M_{B_2} M_{\theta_2}^{-1}.$$

We can interpret $M_\phi^{-1} M_{\theta_1}$ as the phase shift at the first boundary, $M_{\theta_2}^{-1} M_\phi$ as the phase shift at the last boundary and $M_{\theta_1}^{-1} M_{\theta_2}$ as the phase shift at the barrier at $x = 0$. Thus, we can rewrite the above equation as

$$[\,1 \quad r\,]^{\mathrm{T}} = M_A^* {M_\phi}^{-1} T_{\mathrm{DMVP}} M_\phi M_{A^*} [\,t \quad 0\,]^{\mathrm{T}}. \tag{13}$$

The resulting two equations can be solved to yield the transmittance through DMVP barriers, which has been plotted in figure 4.

We shall now discuss similarities between transport of massless Dirac fermions through MVP barriers and electromagnetic propagation in periodic stratified media [23, 24] as

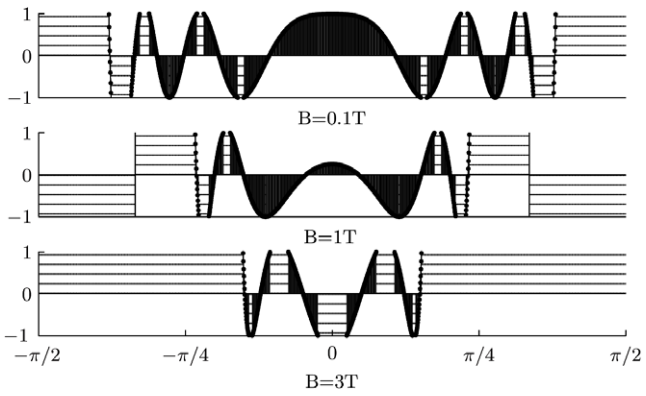

Figure 5. $\cos(KD)$ versus ϕ for an infinite periodic lattice with $d = 100$ nm showing evanescent (dashed) and propagating (solid) Bloch waves. For comparison with earlier plots, ϕ is still used.

well as Dirac fermions in periodic electrostatic potentials [25]. In real structures, there will only be a finite number of barriers and the lattice translational symmetry will break down at the boundary. To simplify the analysis, we assume that the DMVP barrier structure can be repeated infinitely. We consider each unit cell of size $D = 2d$. The nth cell is given by $(n-1)D < x < nD$. In the αth part of the given unit cell, the wavefunction is

$$\phi_1 = a_n^\alpha e^{iq_{\alpha x}^n (x-nD)} + b_n^\alpha e^{-iq_{\alpha x}^n (x-nD)}$$

$$\phi_2 = s_n^\alpha [a_n^\alpha e^{i[q_{\alpha x}^n (x-nD)+\theta_\alpha]} - b_n^\alpha e^{-i[q_{\alpha x}^n (x-nD)+\theta_\alpha]}].$$

Here, $\alpha = 1, 2$, $a_n^1 = a_n$, $b_n^1 = b_n$, $a_n^2 = c_n$, $b_n^2 = d_n$, $q_{1x}^n = q_1$, $q_{2x}^n = q_2$. The exponential factor e^{-inD} reveals the lattice translational symmetry, which is not present for isolated single and double barrier structures. Imposing continuity at both interfaces of the nth unit cell gives

$$\begin{aligned} M_{s_{2,n-1}} M_{\theta_2} \begin{bmatrix} c_{n-1} \\ d_{n-1} \end{bmatrix} &= M_{s_{1,n}} M_{\theta_1} M_{B_1}{}^2 \begin{bmatrix} a_n \\ b_n \end{bmatrix} \\ M_{s_{1,n}} M_{\theta_1} M_{B_1} \begin{bmatrix} a_n \\ b_n \end{bmatrix} &= M_{s_{2,n}} M_{\theta_2} M_{B_2} \begin{bmatrix} c_n \\ d_n \end{bmatrix}. \end{aligned} \tag{14}$$

Imposing the Bloch condition gives the band structure from the following eigenequations

$$\begin{bmatrix} c_n \\ d_n \end{bmatrix} = e^{iKD} \begin{bmatrix} c_{n-1} \\ d_{n-1} \end{bmatrix} = \begin{bmatrix} K_{11} & K_{12} \\ K_{21} & K_{22} \end{bmatrix} \begin{bmatrix} c_{n-1} \\ d_{n-1} \end{bmatrix}$$

where K is the Bloch momentum and the matrix elements K_{ij} can be calculated from equation (14) as

$$\begin{bmatrix} K_{11} & K_{12} \\ K_{21} & K_{22} \end{bmatrix} = (M_{\theta_2} M_{B_2})^{-1} M_{\theta_1} (M_{\theta_1} M_{B_1})^{-1} M_{\theta_2}.$$

This is the same as T_{DMVP}^{-1} permuted. Unitarity gives $\det K_{ij} = 1$, yielding the eigenvalue equation

$$K(\phi, B) = \frac{1}{2d} \cos^{-1} \left[\frac{1}{2} \mathrm{Tr}(K_{ij}) \right].$$

The condition $|\frac{1}{2}\mathrm{Tr}(K_{ij})| < 1$ corresponds to propagating Bloch waves, whereas $|\frac{1}{2}\mathrm{Tr}(K_{ij})| > 1$ leads to evanescent

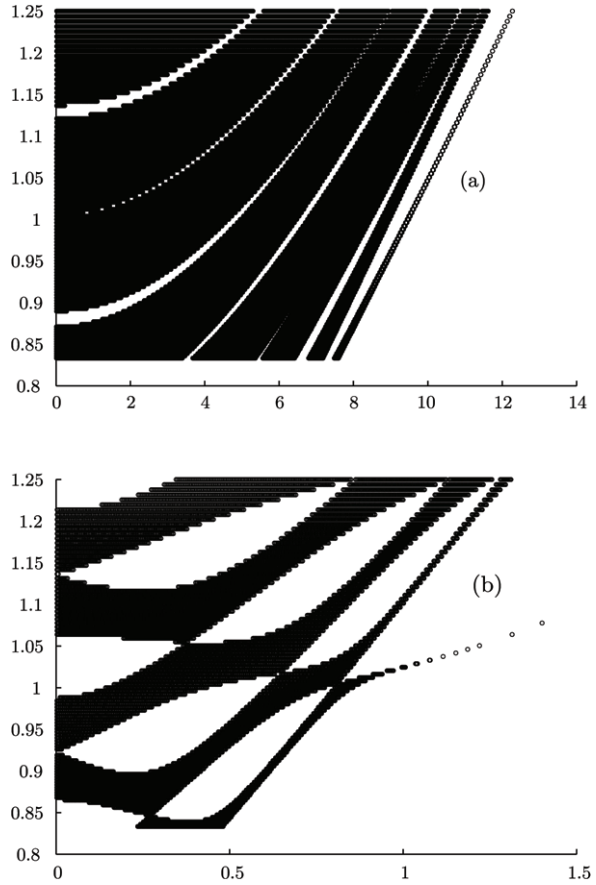

Figure 6. ϵ/ϵ_F versus $k_y l_B$ for an infinite periodic lattice with $d = 100$ nm. Here, ϵ_F is the Fermi level for $\lambda_F = 50$ nm. (a) $B = 0.1$ T, and (b) $B = 3$ T.

Bloch waves that correspond to forbidden zones in the band structure. Such band structures have previously been studied for many problems including condensed matter systems, optics [23, 24] and relativistic quarks [25]. We plot in figure 5 the value $|\frac{1}{2}\mathrm{Tr}(K_{ij})|$ as a function of the incident angle ϕ for different B values. A forbidden region appears at $\phi = 0$ at higher B due to the larger difference between the refractive indices of adjacent regions.

Figure 6 gives the band structure for two different B field values. The most prominent feature of the band structure for the present case is the presence of larger forbidden zones with increasing magnetic field. Such band structures were earlier analyzed for non-relativistic electrons [10, 26], where parabolic spectra were observed. In comparison, in the present case, for low field (figure 6(a)) the forbidden region shrinks substantially whereas for higher field (figure 6(b)) there are large forbidden regions. Similar to the parabolic spectrum, the lower energy bands are of lower width and the higher bands are larger in width.

We shall now modify the above result of infinite periodic barriers to analyze a finite chain of DMVP barriers that make a Bragg reflector. A Bragg reflector can be formed by superposing n such DMVP barriers side by side. We shall briefly describe how the transmittance and reflectance of such a reflector can be calculated using a transfer matrix formalism.

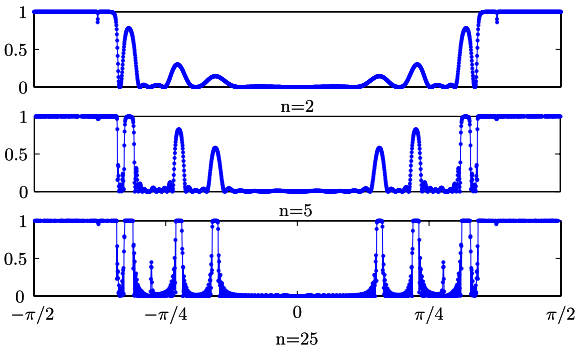

Figure 7. Reflectance versus ϕ through a Bragg reflector with different periods of DMVP barriers of $d = 100$ nm and $B = 0.1$ T.

The magnetic field for a Bragg reflector placed symmetrically around the origin can be written as

$$\boldsymbol{B} = B_z(x)\hat{z} = B\ell_B[\delta(x + nd) + \delta(x - nd) + \sum_{p=1-n}^{n-1}(-1)^{p+n}2\delta(x - pd)]\hat{z}. \quad (15)$$

The series of wavefunction solutions in the various regions are linear combinations of right and left moving waves similar to the ones given earlier in equations (10) and (11) for one DMVP barrier. To solve this set of equations, we proceed as earlier using continuity of the wavefunction at the magnetic barriers at $x = pd, -n \leqslant p \leqslant n$. Just as equation (13) describes the solution for one DMVP barrier, the solutions for n DMVP barriers can be written in matrix form as

$$[\,1 \quad r\,]^{\mathrm{T}} = (M_A{}^{-1})^n M_\phi^{-1} T_{\mathrm{DMVP}}^n M_\phi (M_{A^*})^n\,[\,t \quad 0\,]^{\mathrm{T}}. \quad (16)$$

Here, we have used equation (12) and T_{DMVP} is just the transfer matrix through a DMVP barrier. We can again interpret $M_\phi^{-1}M_{\theta_1}$ as the phase shift at the first boundary and $M_{\theta_2}^{-1}M_\phi$ as the phase shift at the last boundary. These two boundaries are special since these are the interfaces of the magnetic medium with the non-magnetic region. What appears in the middle is the transmission through DMVP barriers repeated n times. A representative plot is given in figure 7. As can be seen, a practical Bragg reflector with a high enough reflectance can be realized with just a few periods of DMVP barriers. A Bragg reflector with large n is broadly similar to an infinite periodic lattice. Particularly at low B (0.1 T) around $\phi = 0$, there is high transmission and $R = 0$ for both structures. Similarly, at high B (3 T), there is strong suppression of transmission near $\phi = 0$ in both cases.

The higher reflectance of a Bragg reflector will strongly suppress transport. We define the average transmission as transmittance $T(\phi)$ multiplied by the x-component of velocity integrated over all angles of incidence for a given B and d such that

$$\langle T(B)\rangle = 2v_F \int_0^{\frac{\pi}{2}} \mathrm{d}\phi\, \cos\phi T(\phi). \quad (17)$$

Figure 8 plots $\langle T(B)\rangle$ for various B and d and shows that transmission is strongly suppressed with increased magnetic field, and this happens within a few periods of the Bragg

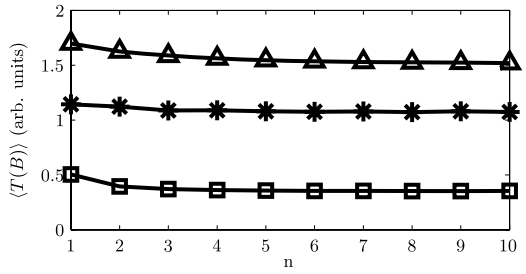

Figure 8. Variation of current $\langle T(B)\rangle$ through a Bragg reflector with period n. $B = 0.1$ T (△), 1 T (∗), 3 T (□) and $d = 100$ nm.

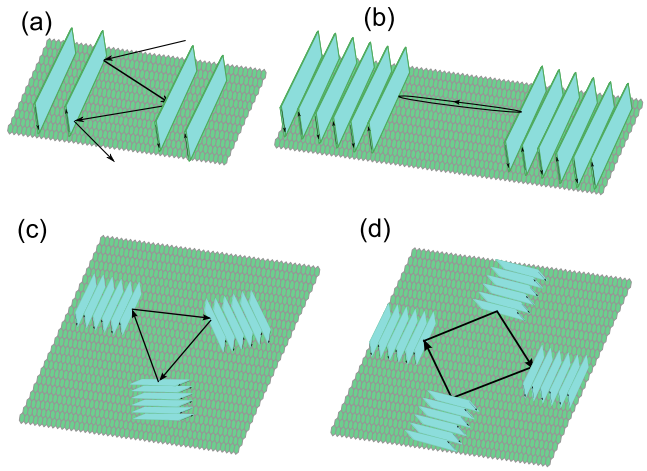

Figure 9. Bragg reflectors with MVP barriers used as a magnetic waveguide (a), and as resonant cavities (b)–(d).

reflector. The above formula, when generalized for a range of energy levels, leads to the conductance of the structure [13, 22], which could be measured experimentally.

We have thus shown that reflectance can be controlled by suitably modifying the strength and locations of the magnetic barriers and thereby changing the refractive index of the intervening medium in a novel manner. This principle could be the basis of more elaborate structures depicted in figure 9. In a magnetic waveguide (figure 9(a)), reflection must be high at the desired propagation angles and could be manipulated by changing the magnetic field. For the resonant cavity shown in figure 9(b), high reflection is needed near normal incidence. Geometries such as three-mirror or four-mirror cavities could be used for high reflection at other angles.

To conclude, we have shown that electron transport through MVP barriers in graphene can be understood in terms similar to light propagation in periodic stratified media. The formalism developed in this paper and the optical analogy can also be helpful in understanding transport for non-relativistic electrons, for which transport through similar magnetic barriers has been previously studied by several researchers such as [13, 27–29]. The formalism describes transport in the ballistic regime, which corresponds to the case of pristine, low-doped graphene. This picture will be modified when the effects of disorder and electron–electron interactions are included.

Using these concepts, practical devices such as Bragg reflectors for manipulating Dirac electrons in graphene can be made. Such barriers suppress Klein tunneling, thereby achieving confinement in graphene which can be seen through strong suppression of transmission of electrons.

We thank G Baskaran, V Fal'ko, C-H Park and F M Peeters for useful comments. The authors acknowledge financial support by IRD Unit, IIT Delhi.

References

[1] Sivan U *et al* 1990 *Phys. Rev.* B **41** 7937
Datta S 2005 *Electronic Transport in Mesoscopic Systems* (Cambridge: Cambridge University Press) chapter 7
[2] Geim A and Novoselov K S 2007 *Nat. Mater.* **6** 183
Novoselov K S *et al* 2004 *Science* **306** 666
Novoselov K S *et al* 2005 *Nature* **438** 197
Zhang Y *et al* 2005 *Nature* **438** 201
[3] Castro Neto A H *et al* 2009 *Rev. Mod. Phys.* **81** 109
[4] Cheianov V V, Fal'ko V and Altshuler B L 2007 *Science* **315** 1252
[5] Veselago V G 1968 *Sov. Phys.—Usp.* **10** 509
Pendry J B 2003 *Nature* **423** 22
[6] Novoselov K S *et al* 2006 *Nat. Phys.* **2** 620
[7] Beenakker C W J 2008 *Rev. Mod. Phys.* **80** 1337
[8] De Martino A, Dell'Anna L and Egger R 2007 *Phys. Rev. Lett.* **98** 066802
[9] Matulis A, Peeters F M and Vasilopoulos P 1994 *Phys. Rev. Lett.* **72** 1518
[10] Ibrahim I S and Peeters F M 1995 *Am. J. Phys.* **63** 171
[11] You J K, Zhang L and Ghosh P K 1995 *Phys. Rev.* B **52** 17243
[12] Zhai F and Chang K 2008 *Phys. Rev.* B **77** 113409
[13] Masir M R *et al* 2008 *Phys. Rev.* B **77** 235443
[14] Masir M R *et al* 2008 *Appl. Phys. Lett.* **93** 242103
[15] Terris B D and Thomson T 2005 *J. Phys. D: Appl. Phys.* **38** R199
Krawczyk M and Puszkarski H 2008 *Phys. Rev.* B **77** 054437
Bader S D 2006 *Rev. Mod. Phys.* **78** 1
[16] Sun S H *et al* 2000 *Science* **287** 1989
[17] Zheng H *et al* 2002 *Appl. Phys. Lett.* **80** 2583
[18] von Bergmann K *et al* 2006 *Phys. Rev. Lett.* **96** 167203
[19] Shon N H and Ando T 1998 *J. Phys. Soc. Japan* **67** 2421
[20] Sharma M and Ghosh S 2009 in preparation
[21] Oroszlàny L *et al* 2008 *Phys. Rev.* B **77** 081403R
Ghosh T K *et al* 2008 *Phys. Rev.* B **77** 081404R
[22] Dell'Anna L and De Martino A 2009 *Phys. Rev.* B **79** 045420
[23] Yeh P, Yariv A and Hong C S 1977 *J. Opt. Soc. Am.* **67** 423
[24] Berreman D W 1972 *J. Opt. Soc. Am.* **62** 502
[25] McKellar B H J and Stephenson G J Jr 1987 *Phys. Rev.* C **35** 2262
Mendez B *et al* 1993 *J. Phys. A: Math. Gen.* **26** 171
Strange P 1998 *Relativistic Quantum Mechanics* (Cambridge: Cambridge University Press)
Cheianov V V and Fal'ko V 2006 *Phys. Rev.* B **74** 041403
Barbier M *et al* 2008 *Phys. Rev.* B **77** 115446
Park C-H *et al* 2008 *Nat. Phys.* **4** 213
[26] Krakovsky A 1996 *Phys. Rev.* B **53** 8469
[27] Reijniers J, Peeters F M and Matulis A 2001 *Phys. Rev.* B **64** 245314
[28] Reijniers J and Peeters F M 2001 *Phys. Rev.* B **63** 165317
[29] Papp G, Vasilopoulos P and Peeters F M 2005 *Phys. Rev.* B **72** 115315